Supplementary information: Continuous carbon nanotube synthesis on charged carbon fibers

David B. Anthony[a, b, c], XiaoMeng Sui[d], Israel Kellersztein[d], Hugo G. De Luca[a], Edward R. White[a], H. Daniel Wagner[d], Emile S. Greenhalgh[c], Alexander Bismarck[b, e], Milo S. P. Shaffer[a,*]

[a] Nanostructured Hierarchical Assemblies and Composites (NanoHAC) Group, Department of Chemistry, Imperial College London, South Kensington Campus, London SW7 2AZ, UK
[b] Polymer and Composite Engineering (PaCE) Group, Department of Chemical Engineering, Imperial College London, South Kensington Campus, London SW7 2AZ, UK
[c] The Composites Centre, Department of Aeronautics, Imperial College London, South Kensington Campus, London SW7 2AZ, UK
[d] Department of Materials and Interfaces, Weizmann Institute of Science, Rehovot 76100, Israel
[e] Polymer and Composite Engineering (PaCE) Group, Institute of Materials Chemistry and Research, Facility of Chemistry, University of Vienna, Währinger Str. 42, A-1090 Vienna, Austria

[*] Corresponding author: Fax: +44 (0)20 7594 5801, E-mail address: m.shaffer@imperial.ac.uk (M.S.P. Shaffer)

Contents

S1 Model “ideal” perpendicular CNT length for composites reinforced with carbon nanotube-grafted-fiber 3
S2 Continuous chemical vapor deposition (CVD) set-up equipment details 4
S2.1 Lenton furnace and thermometer 4
S2.2 Quartz tubes and fittings 4
S2.3 Motor, friction drive and creel 4
S2.4 Power supply and electrical connections 4
S2.5 Mass flow controllers 4
S2.6 Furnace profile of stable temperature zone 5
S2.7 Schematic of concentric tube arrangement including gas inlet/outlets 5
S3 Considerations for use of combustible gases in open chemical vapor deposition-reactor 6
S4 Potential difference applied during continuous carbon nanotube-grafted-carbon fiber (CNT-g-CF) synthesis 7
S5 Single fiber pull-out Embedding and test equipment 8
S5.1 Single fiber pull-out equipment details 8
S6 Additional scanning electron micrographs 9
S7 Baseline samples subjected to elevated temperature and reductive conditions with applied potential difference (p.d.). 12
S8 Baseline samples subjected to elevated temperature and reductive conditions without applied potential difference (p.d.) 13
S9 Single fiber tensile test tabulated data 14
S10 Single fiber fragmentation test tabulated data 15
S11 Single fiber pull-out test 16
S12 Brunauer, Emmett and Teller (BET) isotherms 19
S13 Raman analysis 20
S14 Thermogravimetric analysis and derivatives 21
S14.1 Determining temperature combustion onset 22
S15 Continuous CVD carbon nanotube-grafted-carbon fiber with sequentially altered potential difference 23
Appendix acronyms and symbols 25
Acknowledgements 25
Appendix references 26

S1 Model "ideal" perpendicular CNT length for composites reinforced with carbon nanotube-grafted-fiber

A calculation to determine carbon fiber reinforced composite's (CFRC's) ideal packing fiber volume fraction, in a hexagonal arrangement, with a representative composite fiber-matrix composition of 60 vol.% fiber reinforcement and 40 vol.% matrix, with no voids. An idealized CFRC fiber separation in such an arrangement is shown below (Figure S.1).

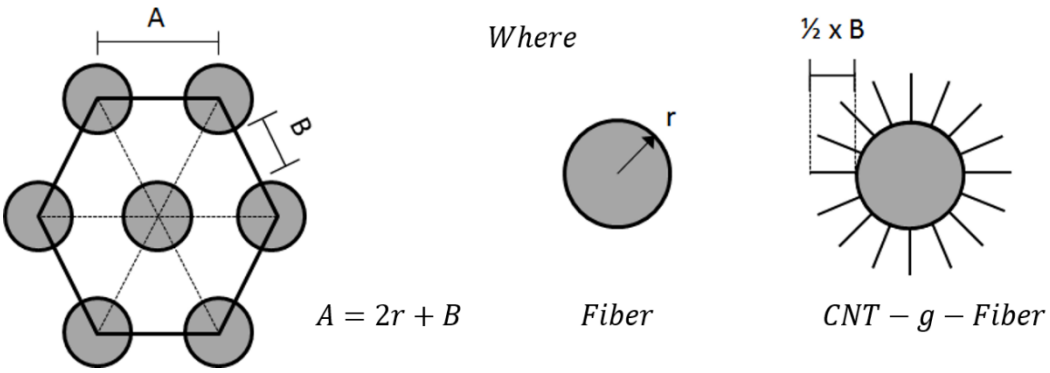

Figure S.1 A schematic of a CFRC with regular hexagonal packing arrangement and the proposed inclusion of carbon nanotube-grafted-fiber (CNT-g-F), which in this instance, the carbon nanotubes (CNTs) from one fiber just touch the adjacent CNTs of another. CNTs with length (½ B) from fiber surface would produce a hierarchical composite with the same packing density and arrangement of reinforcing elements. Distance from fiber-fiber center indicated as A, and separation between fibers shown as B in the figure.

- $Area\ of\ hexagon = 6\ \times area\ of\ triangle = \frac{3\sqrt{3}}{2}A^2 = 0.6\ fiber\ area + 0.4\ matrix\ area$
- $3\ fibers\ within\ hexagonal\ unit\ cell = 3\pi r^2 = 0.6\ fraction\ of\ area$
- $So\ 0.4\ matrix\ area = \frac{2}{3}\times\ 3\pi r^2 = 2\pi r^2$
- $\therefore Area\ of\ hexagon = 5\pi r^2 = \frac{3\sqrt{3}}{2}A^2$
- $A = \sqrt{\left(\frac{10}{3\sqrt{3}}\pi r^2\right)}$
- $B = A - 2r$
- $When\ r = 3.55\ \mu m$
  $(typical\ fiber\ diameter\ in\ this\ instance\ AS4\ carbon\ fiber\ (Hexcel)\ is\ 7.1\ \mu m)$[†]
- $A = 8.7\ \mu m\ (seperation\ including\ radius\ of\ fibers)$
- $B = 1.6\ \mu m\ (seperation\ bewteen\ fibers)$

- *The CNT length from the fiber surfaces which results in adjacent fibers just touching CNTs* $= \frac{1}{2}B = 0.8\ \mu m\ at\ 60\ vol\%\ fibre\ composition$
- *The general form for maximum distance between two fibers at a given volume fraction in a hexagonal close packing arrangement is;*
  $B = r\left(\sqrt{\frac{2\pi}{V_f\sqrt{3}}} - 2\right)$ *where* V_f *is fiber volume fraction*

[†] Hexcel Composites, HexTow™ AS4 Carbon Fiber. Data Sheet 2009

S2 Continuous chemical vapor deposition (CVD) set-up equipment details

S2.1 Lenton furnace and thermometer

- PTF 15//610, Lenton, GB.
- Temperature probe: KHXL-IM30U-RSC-1000, Omega Engineering Ltd, GB.
- Thermometer: KM330 Single Channel, Temperature range, -50 °C to 1300 °C, accuracy, 0 to 1100 °C ± (0.2% of reading +1) °C, Kane-May by Comark, GB.

S2.2 Quartz tubes and fittings

- Quartz tubes sourced from Robson Scientific, GB. Note that the position of the small tubes could be varied.
- Outer tube, 51.0 ± 0.5 mm outer diameter (OD), 2.5 ± 0.2 mm wall thickness, 1600 mm in length.
- Middle tube, 25.0 ± 0.2 mm OD, 1.5 ± 0.2 mm wall thickness, 610 mm in length
- Small tube (left), 19.0 ± 0.3 mm OD, 1.5 ± 0.2 mm wall thickness, 650 mm in length.
- Small tube (right), 19.0 ± 0.3 mm OD, 1.5 ± 0.2 mm wall thickness, 680 mm in length.

- Quick connect tube adaptors: bespoke concentric and cantilevered arrangement, stainless steel, LewVac LLP, GB. A variation of the stock item Hybrid Adapters: Quick Connect Adapters. The connection of the metal sleeve to the quartz tube is made using an O-ring seal to the outer surface of the quartz tube.

S2.3 Motor, friction drive and creel

- Electrical motor: Crouzet, 828600, 1.5 rpm with associated friction belt drive.
- Creel structure: aluminum profiles bought from RS Components Ltd, GB, assembled in bespoke design by Imperial College London, Chemical Engineering Workshop, GB.

S2.4 Power supply and electrical connections

- Power supply: Mastech HY3003D, 30 V max, 3 A max, Digimess Instruments Ltd, GB.
- High voltage amplifier: MM3P1.5/12, 3 kV max, 0.5 mA max, 1:250, Spellman High Voltage Electronics, GB.
- High voltage probe: TT-HVP 40, 1000:1 divider, division ratio accuracy 1%, Testec, DE.
- Multimeter: IDM67, ± 0.7% voltage, ± 1.0% current, IEC 1010-1 CAT II 600V, ISO-Tech, GB.
- Steel pin electrode: ½" stainless steel tubing, Swagelok Company, US.
- Graphite foil counter electrode: 99.8%, C1179, Advent Research Materials Ltd, GB, approximate dimensions 100 mm x 180 mm x 0.2 mm.
- Ceramic fish spine beads: 536-4062, RS Components Ltd, GB.

S2.5 Mass flow controllers

Bronkhorst digital mass flow controllers;

- Nitrogen: F-201CV-5K0-RAD-22-V, EL-FLOW Select, max flow 7500 sccm, ±0.5% reading plus ±0.1% full scale.
- Nitrogen with 2.4 vol.% hydrogen: F-201CV-5K0-RAD-22-V, EL-FLOW Select, max flow 3400 sccm, ±0.5% reading plus ±0.1% full scale.
- Nitrogen with 1.3 vol.% acetylene: F-201CV-500-RAD-22-V EL-FLOW Select, max flow 325 sccm, ±2% full scale.

Mass flow controllers used a computer interface, software FlowDDE V4.62 MBC Flow-Bus host with FlowView 10 V1.17, Bronkhorst UK Ltd, GB.

S2.6 Furnace profile of stable temperature zone

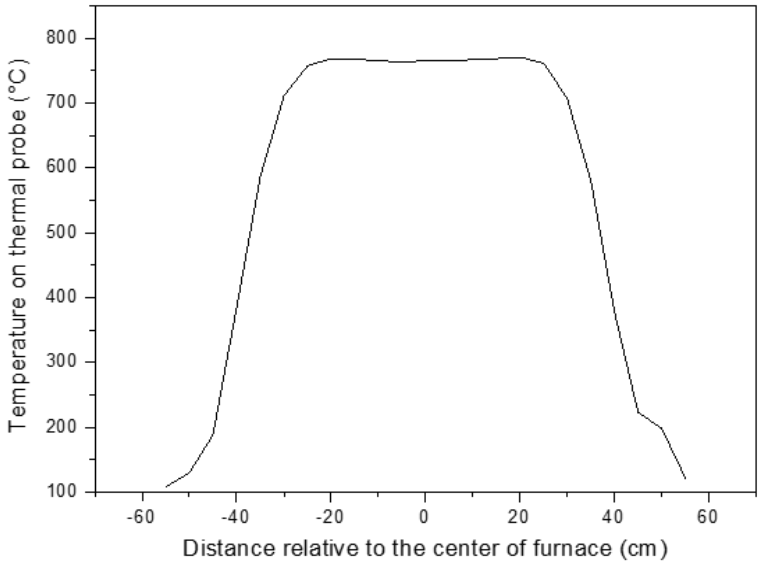

Figure S.2 Temperature profile inside the open 2" quartz tube inside furnace, furnace set to reaction temperature 770 °C.

S2.7 Schematic of concentric tube arrangement including gas inlet/outlets

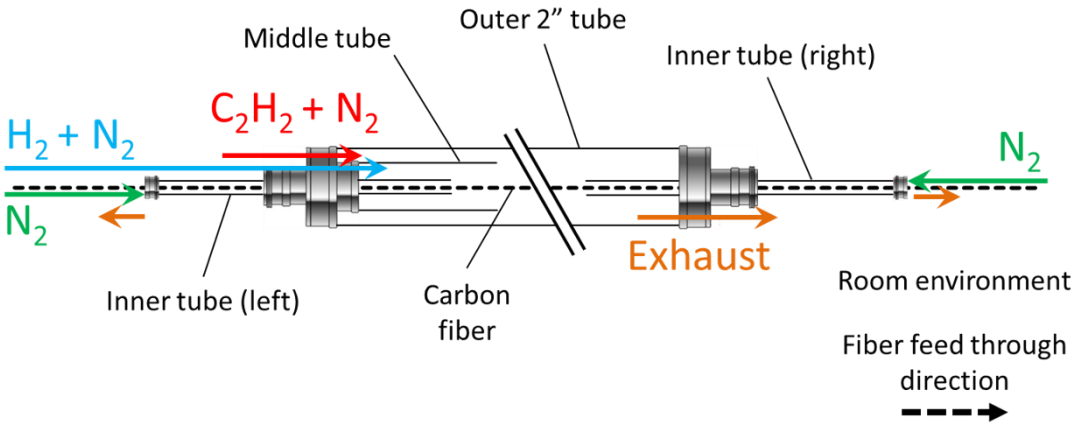

Figure S.3 Schematic of the concentric quartz tubes which determine the reaction regions shown in Figure 2 (c) in the main text, with reactor gas inlet/outlets highlighted.

S3 Considerations for use of combustible gases in open chemical vapor deposition-reactor

The use of flammable gases, acetylene and hydrogen, in an open chemical vapor deposition reactor requires careful consideration. T_{ci} values are defined as "the maximum flammable gas content for which a mixture of the flammable gas *i* in nitrogen is not flammable in air, in percent by volume (or mol.%)".[1] Note that the inerting capacity of nitrogen is higher than that of argon for flammable gases,[1] subsequently a higher vol.% of flammable gases in nitrogen mix can be achieved. Inert gases, inherently, only act as a carrier gas in CVD-synthesis therefore it was assumed that choice of inert gas should not affect CNT growth. T_{ci} values for acetylene and hydrogen at standard ambient temperature and atmospheric pressure in air are 3.0 vol.% and 5.5 vol.%, respectively, Table S.1.[1-3] The T_{ci} of flammable gases are dependent on the temperature and pressure, with permissible vol.% decreasing with increasing temperature. N.b. the continuous CVD system operates at significantly high temperatures above ambient and auto-ignition, 296 °C for acetylene and 570 °C for hydrogen in air. T_{ci} values are not described in literature at elevated temperatures for acetylene nor hydrogen. Examples of the temperature effect on T_{ci} values for alkanes, are however, available.[4]

Table S.1 Flammable gas properties and T_{ci} values from literature. Boiling point (BP), T_{ci} at standard ambient temperature and atmospheric pressure (SATP),[1-3] adiabatic flame temperature at constant pressure (AFTCP) generated using CERFACS,[5] and auto ignition temperature (AIT). BP and AIT are taken from relevant MSDS published by Linde Gas North America LLC.

Gas	BP	T_{ci} at in air at SATP (20 °C)	AFTCP	AIT
	[°C]	[vol %]	[°C]	[°C]
Hydrogen	-252.8	5.5	2094	570
Acetylene	-83.8	3.0	2258	296

S4 Potential difference applied during continuous carbon nanotube-grafted-carbon fiber (CNT-g-CF) synthesis

The electrical connection to carbon fibers were made by passing the fibers over a simple pin (shown in main text Figure 2 (a) and (b)), with the counter electrode (graphite foil) mounted towards the reactor exit, with the gas sleeve quartz tube acting as an insulating element.

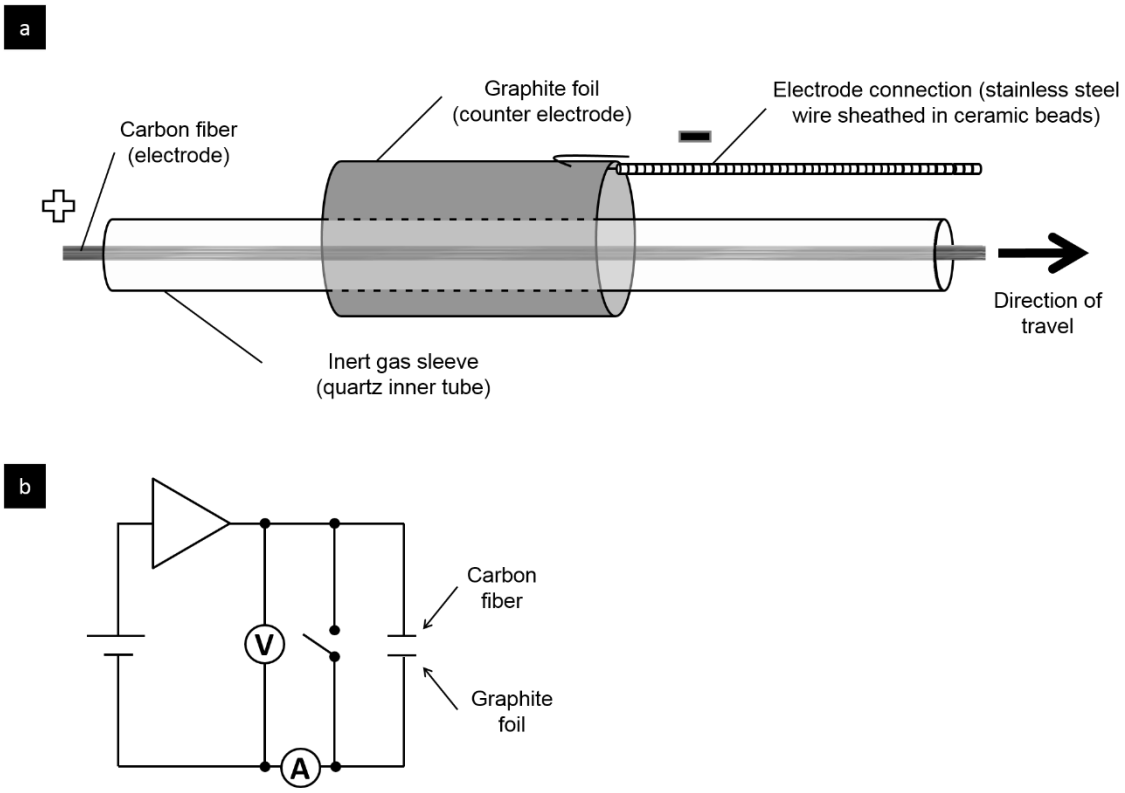

Figure S.4 (a) Enlarged schematic of the electrode arrangement of the co-axial capacitor arrangement inside the reactor, including the connection made to graphite foil with stainless steel wire and ceramic beads to prevent shorting. (b) Circuit diagram, the inclusion of the switch is to ensure complete discharge from the set-up at the end of the experiment.

S5 Single fiber pull-out Embedding and test equipment

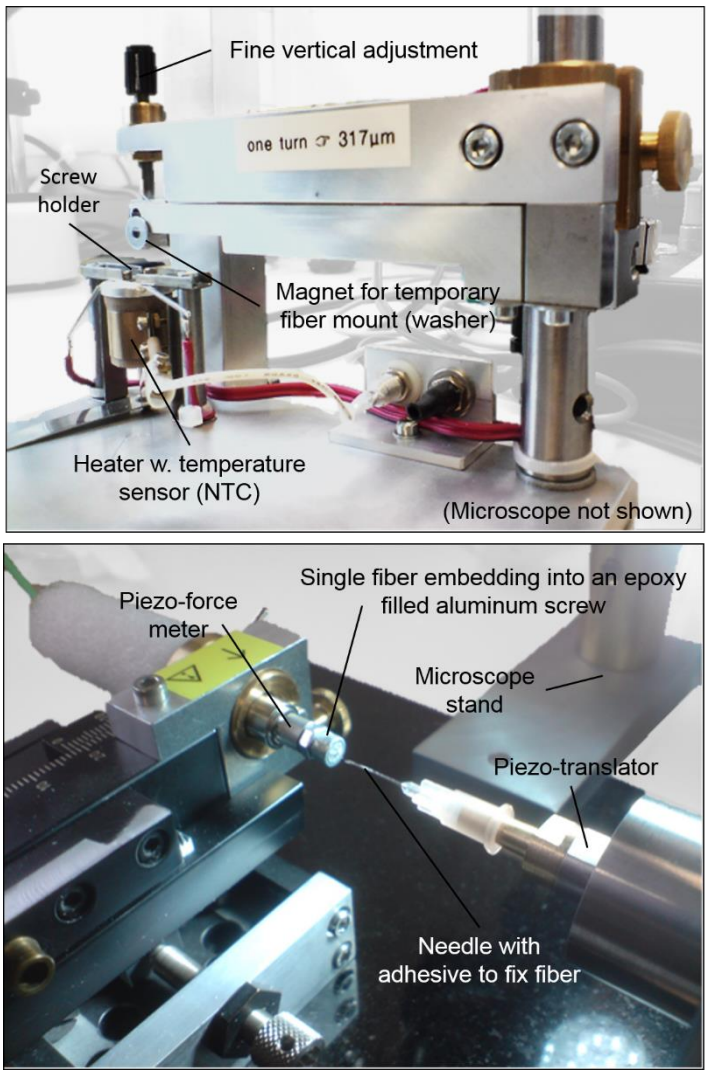

Figure S.5 Single fiber embedding equipment with heater (top), and single fiber pull-out equipment with embedded fiber *in-situ* (bottom).

S5.1 Single fiber pull-out equipment details

- Piezo-actuator: P-216.9S, Preloaded PICA Piezo Actuator, 180 µm, 1000 V, 4500 N with nanoprecision HVPZT-Amplifier unit and PZT-Servo Controller by Physik Instrumente (PI) GmbH & Co. KG, DE.
- Piezo-force sensor: Type 9207, 1-Component Quartz Force Link, Low Force with Miniature Charge Amplifier Type 5030A, Kistler, CH.
- Microscope: stereo, SMZ-140 Series, Motic, DE.
- Computer software and interface: SFPO computer program for controlling the pull-out test developed at BAM using an ADwin-Light-16 PCI interface by Jäger Computergesteuerte Messtechnik GmbH, DE.
- Adhesive to attach the embedded fiber to the needle was Cyanoacrylate adhesive - Type CN, Tokyo Sokki Kenkyujo Co., Ltd, JP.

Single fiber pull-out and single fiber embedding equipment produced by Gerhard Kalinka, Ruediger Sernow and Martina Bistritz, Bundesanstalt für Materialforschung und – prüfung (BAM).

S6 Additional scanning electron micrographs

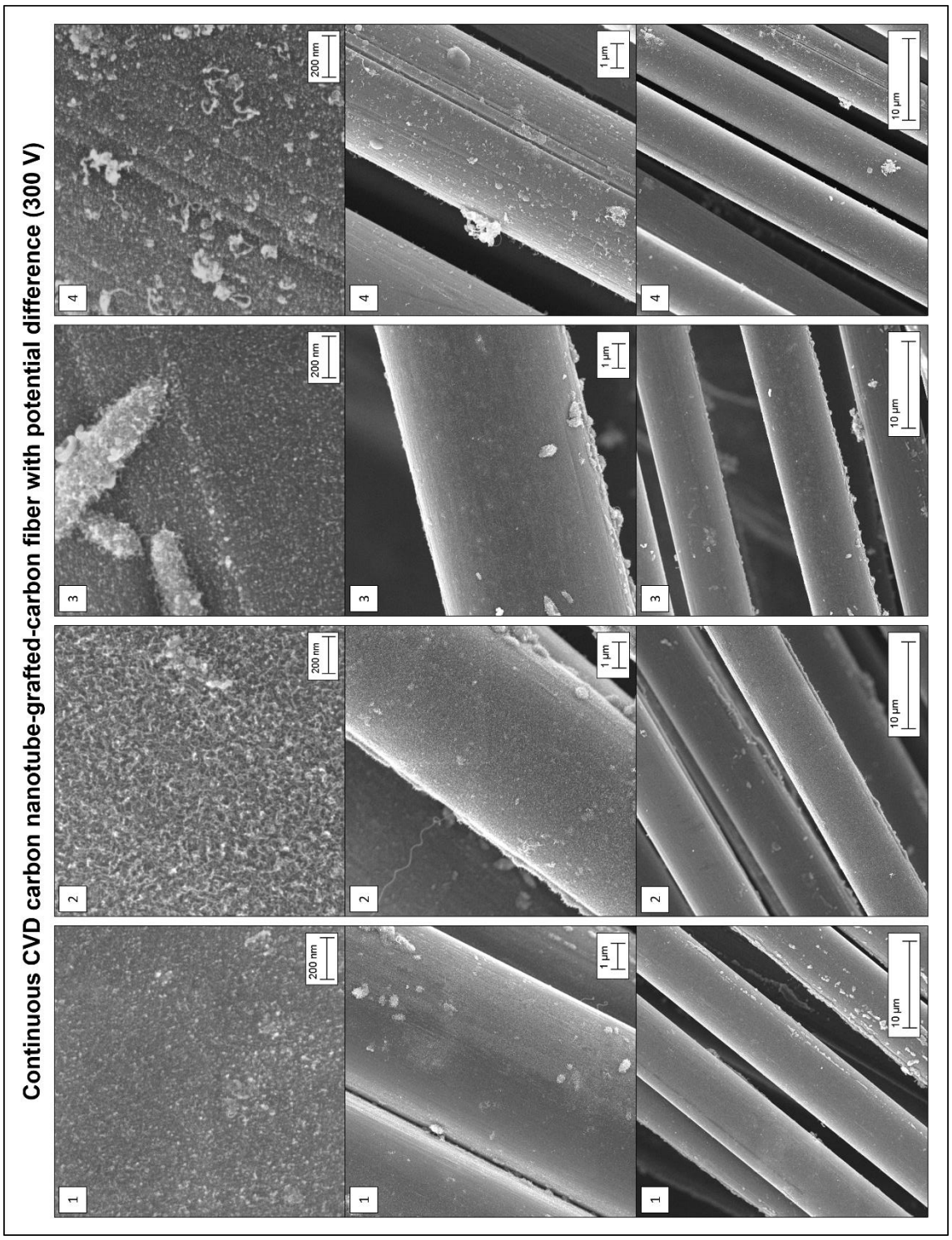

Figure S.6 SEM images of continuous CVD CNT produced with (300 V) an applied potential difference. The columns show different tow regions each separated by at least 0.4 m over a length of 2 m.

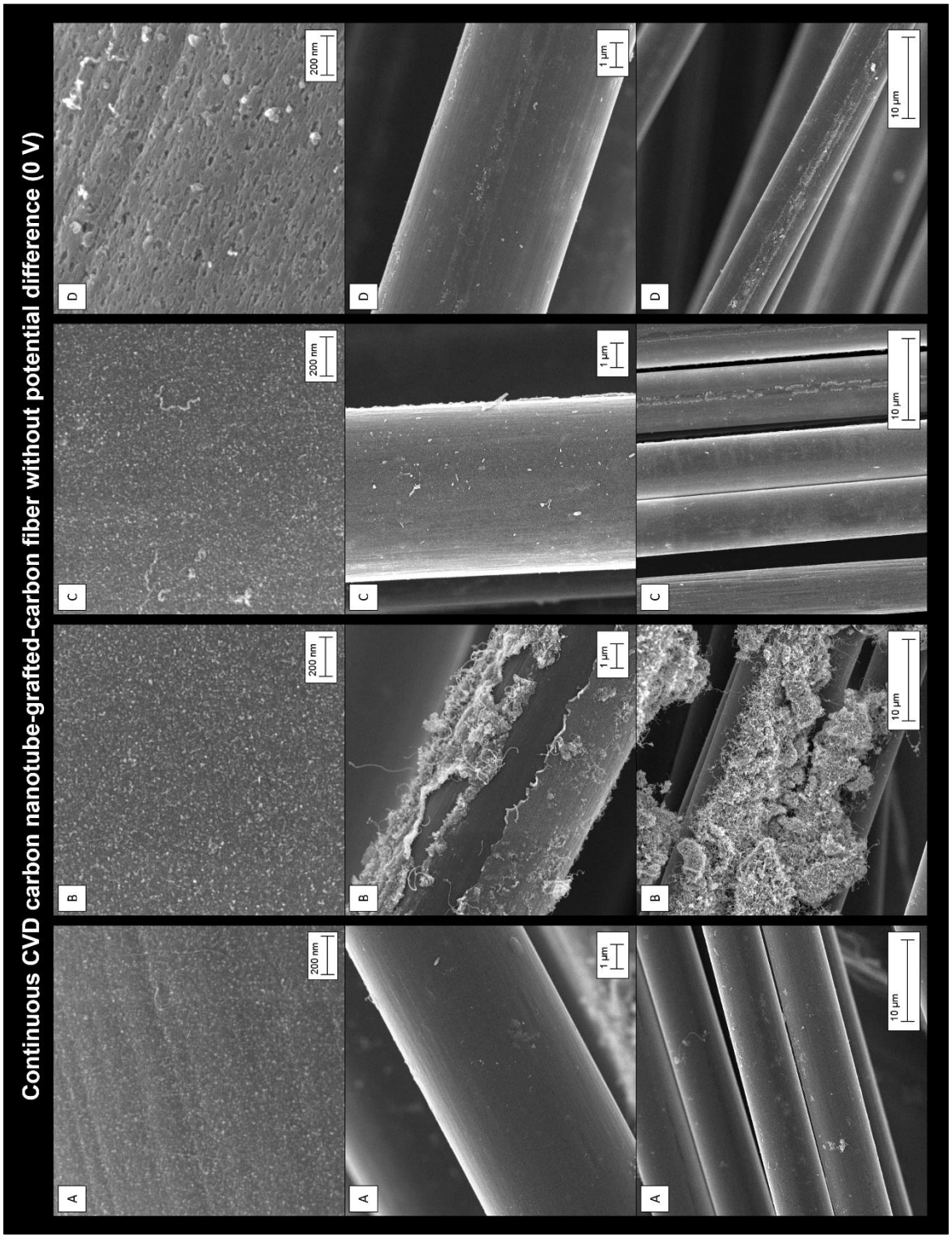

Figure S.7 SEM images of continuous CVD CNT produced without (0 V) an applied potential difference. The columns show different tow regions each separated by at least 0.4 m over a length of 2 m.

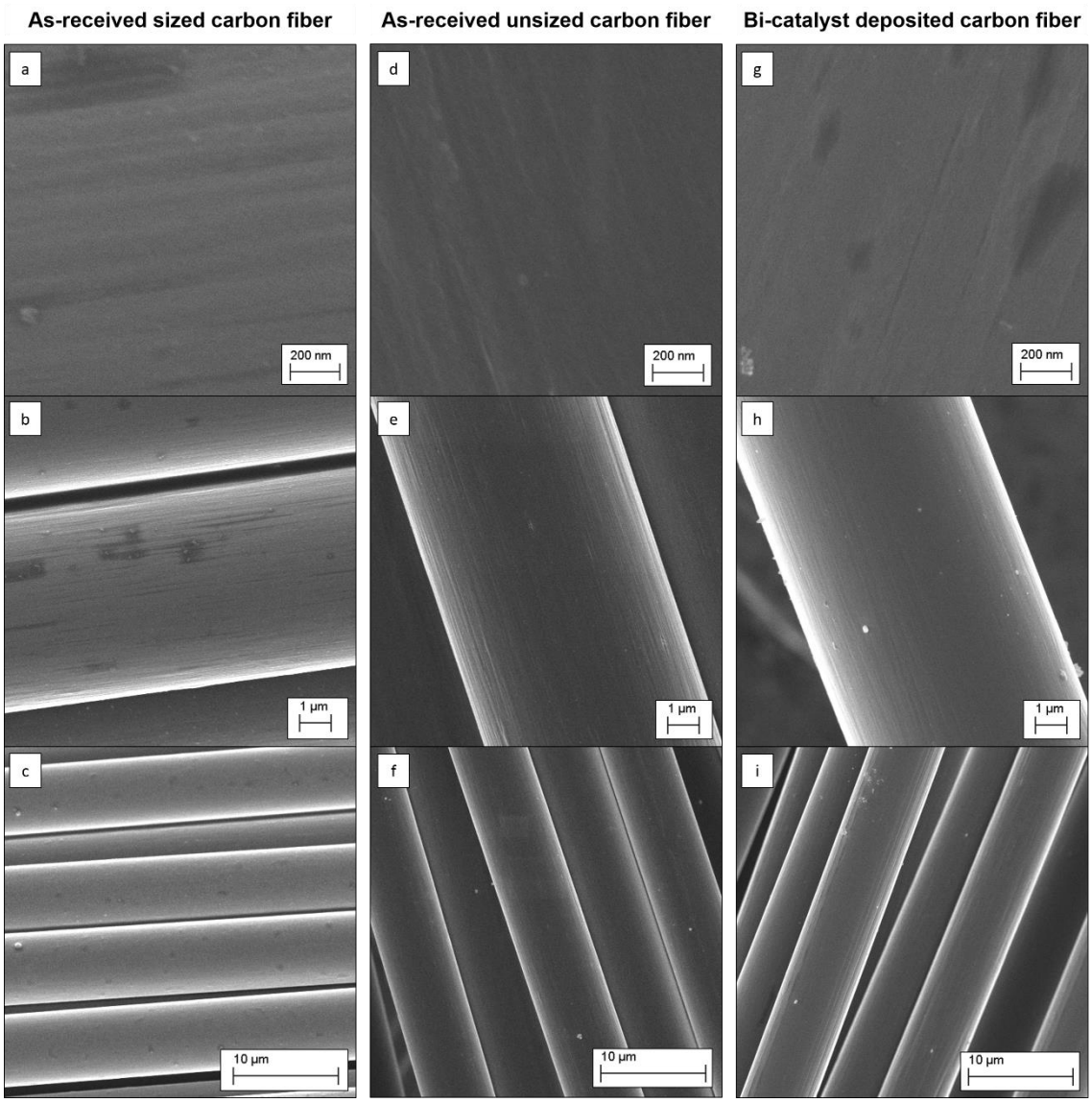

Figure S.8 Scanning electron microscopy (SEM) images (a) to (c) as-received sized carbon fiber, (d) to (f) as-received unsized carbon fiber and (g) to (i) carbon fibers deposited with nickel and iron bi-catalyst precursor.

S7 Baseline samples subjected to elevated temperature and reductive conditions with applied potential difference (p.d.).

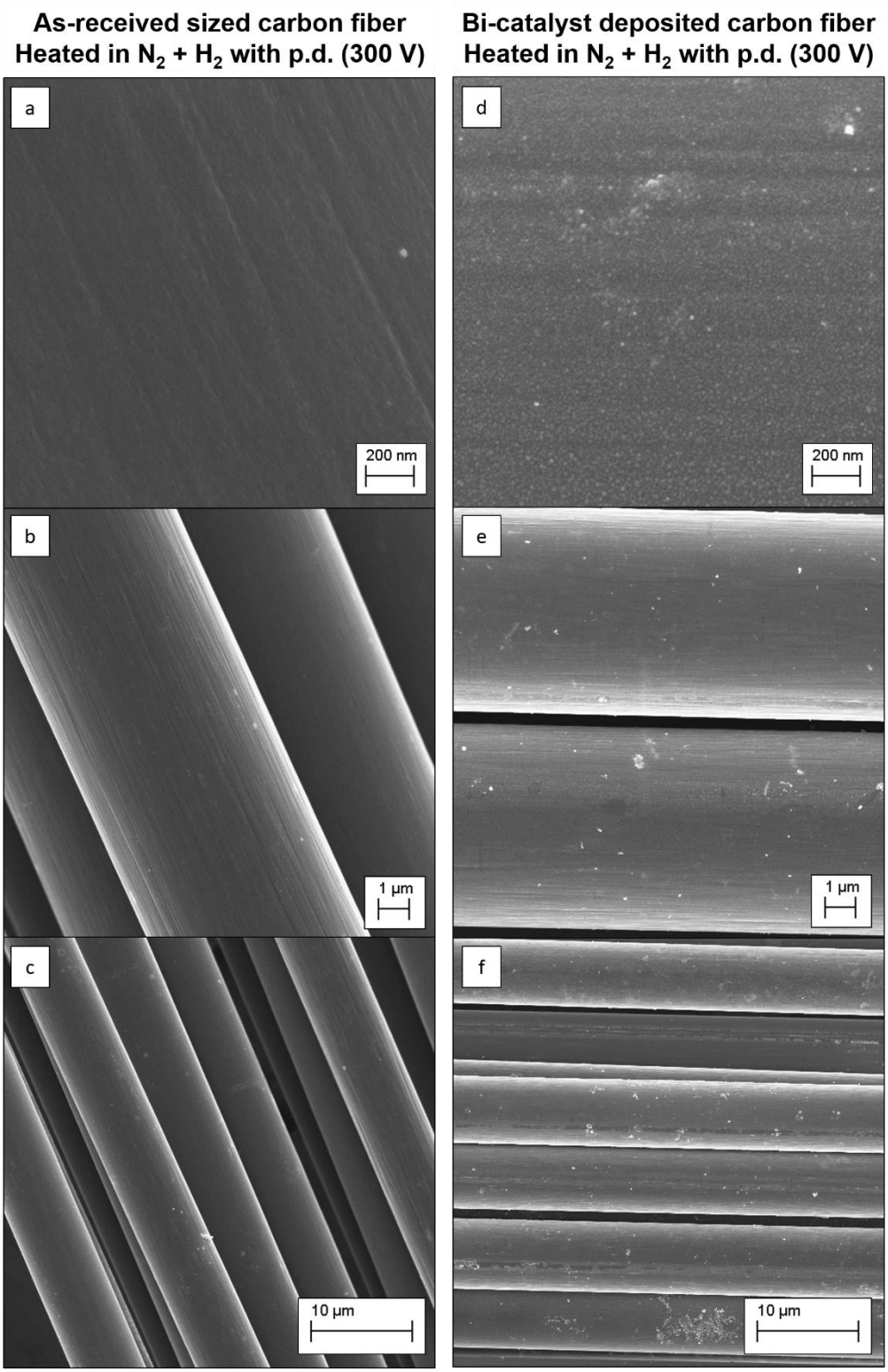

Figure S.9 SEM images (a) to (c) as-received sized carbon fiber, (d) to (f) carbon fibers deposited with nickel and iron bi-catalyst heated at elevated temperatures of 770 °C under reductive conditions in the continuous CVD reactor with an applied potential difference of 300 V.

S8 Baseline samples subjected to elevated temperature and reductive conditions without applied potential difference (p.d.)

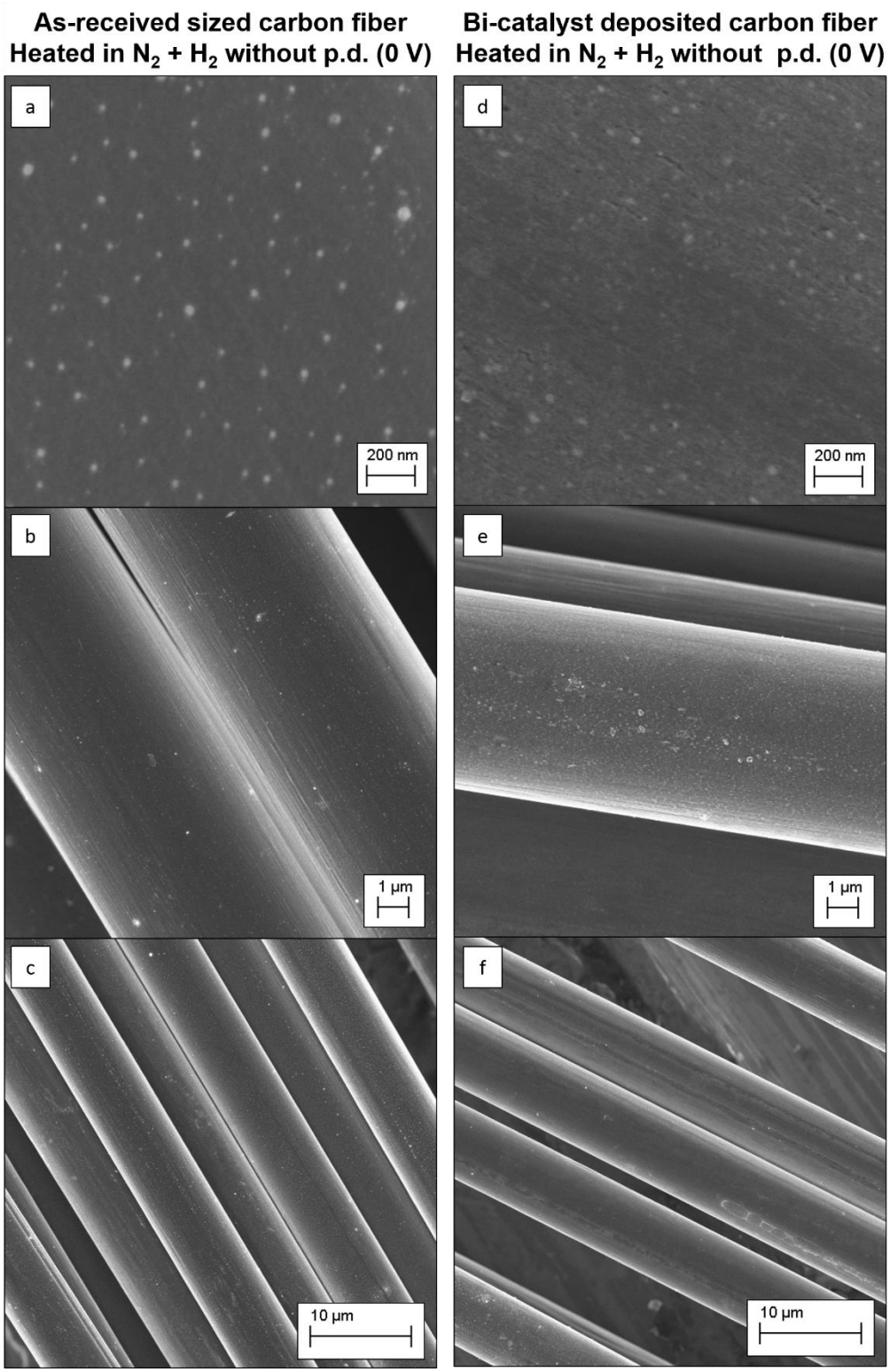

Figure S.10 SEM images (a) to (c) as-received sized carbon fiber, (d) to (f) carbon fibers deposited with nickel and iron bi-catalyst heated at elevated temperatures of 770 °C under reductive conditions in the continuous CVD reactor without an applied potential difference (0 V).

S9 Single fiber tensile test tabulated data

Table S.2 Single fiber tensile test results including values for calculated Weibull shape and scalar parameters.

Carbon fiber sample	Gauge length [mm]	Tensile strength (σ_t) [MPa]	Tensile modulus (E_t) [GPa]	Number of samples tested	Number of samples discarded	Weibull scalar parameter (α) [GPa]	Weibull shape parameter (β)	Average fiber diameter (d) [µm]
As-received sized[6]	15	3453 ± 202	221 ± 2	31	0	8.5	3.4	6.9
	25	2833 ± 121	216 ± 2	30	6	5.7	5.2	
	35	2370 ± 115	220 ± 2	30	0	6.2	4.1	
As-received unsized	15	3807 ± 152	239 ± 6	41	18	6.9	5.3	7.1
	25	3861 ± 157	227 ± 4	35	12	7.0	6.2	
	35	3465 ± 160	236 ± 6	35	14	7.4	5.3	
Bi-catalyst precursor deposition[6]	15	3480 ± 136	212 ± 3	35	7	6.0	5.8	6.9
	25	3049 ± 123	212 ± 3	34	9	5.9	5.5	
	35	2986 ± 115	222 ± 3	35	1	6.3	5.3	
Continuous CNT-g-CF (0 V)	15	2763 ± 101	209 ± 3	34	8	4.7	5.9	6.9
	25	2600 ± 61	209 ± 3	35	6	4.0	8.4	
	35	2371 ± 95	217 ± 3	33	8	4.5	6.2	
Continuous CNT-g-CF (300 V)	15	3030 ± 55	214 ± 3	34	9	4.0	11.2	7.0
	25	2937 ± 59	213 ± 3	32	5	4.0	11.6	
	35	2858 ± 55	225 ± 3	35	8	4.1	11.2	

S10 Single fiber fragmentation test tabulated data

Table S.3 Mechanical properties of single-fiber fragmentation tests in an epoxy matrix.

Carbon fiber sample	Interfacial shear strength (τ_i) [MPa]	Ultimate fiber strength at critical length $\sigma_f(l_c)$ [GPa]	Critical length (l_c) [µm]	Tensile modulus (E) [GPa]	Weibull scalar parameter (α) [GPa]	Weibull shape parameter (β)	Average fiber diameter (d_f) [µm]
As-received sized	102.6 ± 7.7	10.3 ± 0.3	354.6 ± 30.6	1.17 ± 0.12	10.1 ± 0.3	32.1 ± 13.2	7.0
As-received unsized	58.7 ± 2.9	10.5 ± 0.3	629.8 ± 33.1	1.20 ± 0.07	10.6 ± 0.3	17.5 ± 3.7	7.2
Bi-catalyst precursor deposition	46.4 ± 5.5	11.0 ± 1.2	836.4 ± 69.2	1.21 ± 0.12	11.2 ± 1.3	31.0 ± 13.8	6.7
Continuous CNT-g-CF (0 V)	70.6 ± 12.6	10.6 ± 1.2	534.2 ± 93.6	1.08 ± 0.11	10.4 ± 1.0	11.9 ± 5.8	7.0
Continuous CNT-g-CF (300 V)	100.6 ± 5.1	10.1 ± 0.4	351.0 ± 19.7	1.12 ± 0.04	9.6 ± 0.3	12.6 ± 2.6	7.0

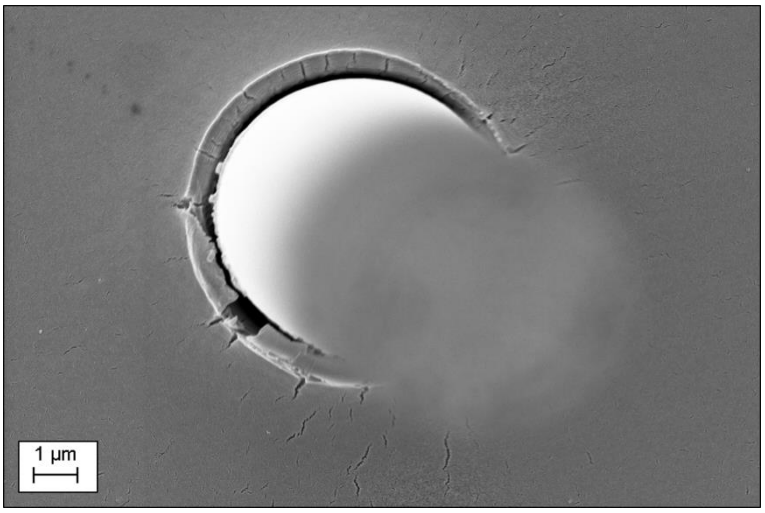

Figure S.11 Single fiber fragmentation fracture surface for bi-catalyst precursor deposition carbon fiber sample.

S11 Single fiber pull-out test

Table S.4 Mechanical properties of single-fiber pull-out tests in an epoxy matrix.

Carbon fiber sample	Interfacial shear strength (τ_{app}) [MPa]	Range of embedded length (l_e) [µm]	Range of maximum force (F_{max}) [mN]	Number of samples tested	Number of samples discarded	Average fiber pull-out diameter (d_f) [µm]
As-received sized	79.7 ± 2.5	47.7 to 107.2	65 to 186	18	3	6.9
As-received unsized	68.5 ± 2.1	51.0 to 122.8	55 to 207	16	1	7.1
Bi-catalyst precursor deposition	71.4 ± 1.8	41.7 to 114.7	62 to 184	17	1	6.9
Continuous CNT-g-CF (0 V)	68.8 ± 1.8	26.0 to 129.9	39 to 225	16	0	6.9
Continuous CNT-g-CF (300 V)	73.3 ± 1.6	30.8 to 88.8	47 to 165	19	1	7.0

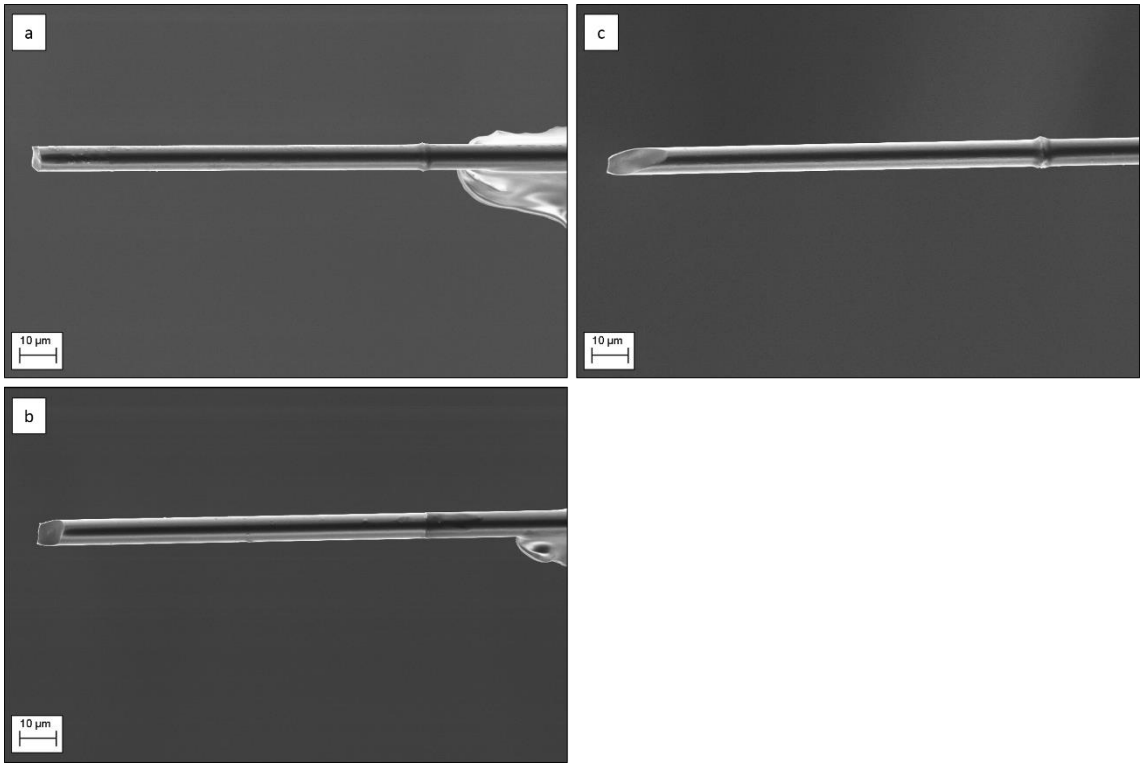

Figure S.12 Single fiber pull-out surfaces, (a) Continuous CNT-g-CF (0 V), (b) as-received unsized, and (c) bi-catalyst precursor deposition carbon fiber, (d) Continuous CNT-g-CF (300 V) with carbon nanotubes highlight under the surface epoxy, N.B. The fibers in all instances have not been coated in SEM preparation.

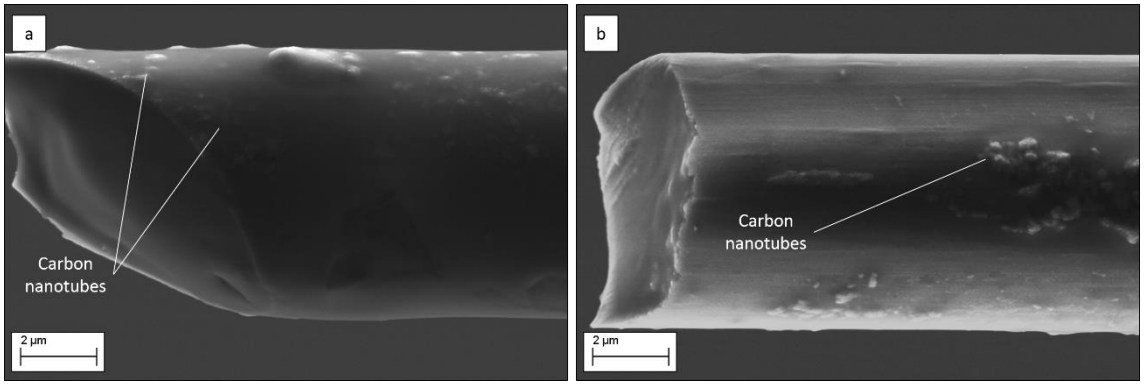

Figure S.13 Single fiber pull-out surfaces, (a) continuous CNT-g-CF (300 V) and (b) continuous CNT-g-CF (0 V) with carbon nanotubes highlight under the surface epoxy, N.B. The fibers in both instances have not been coated in SEM preparation.

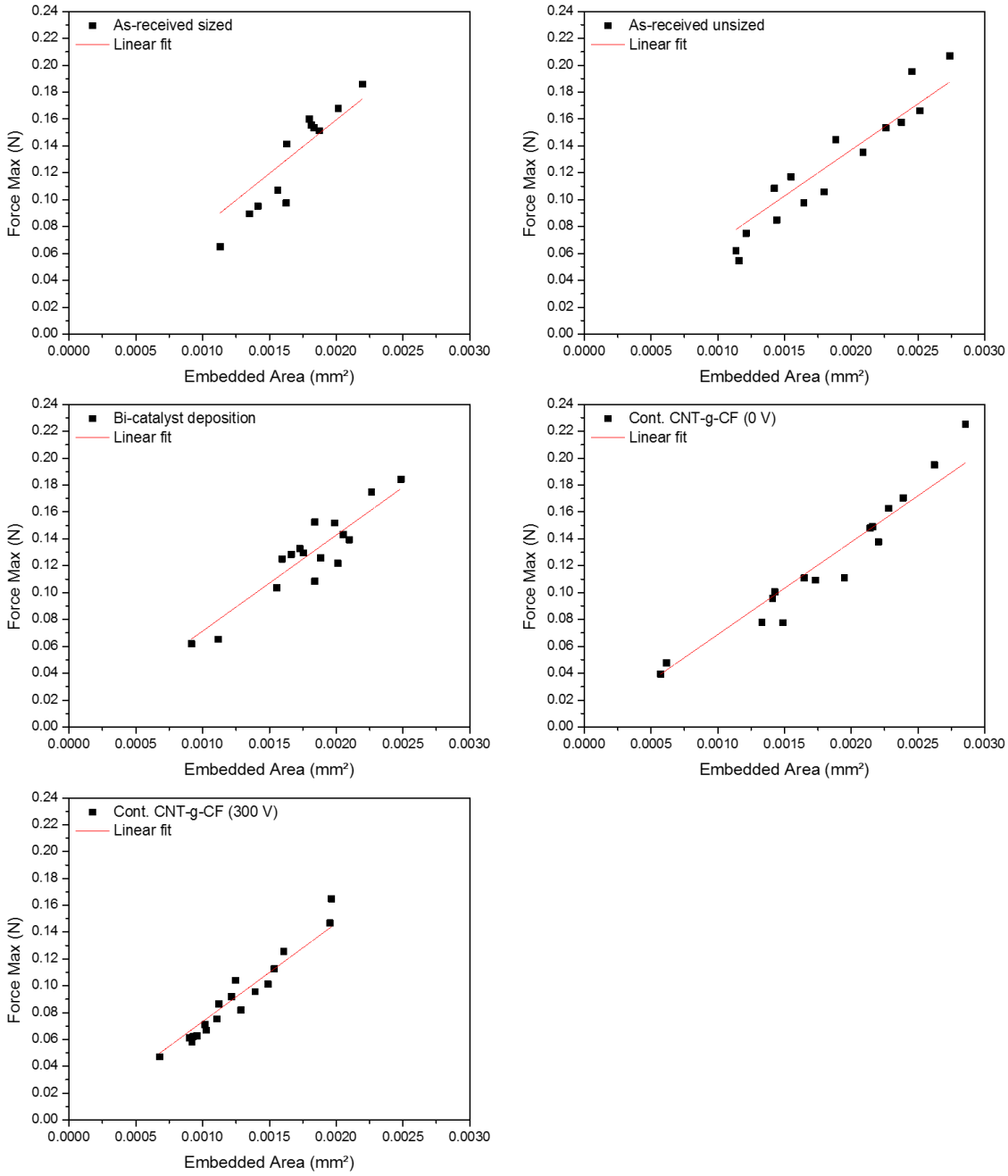

Figure S.14 Single fiber pull-out tests results including a gradient of linear fits which corresponds to the average apparent interfacial shear strength (IFSS) as tabulated in Table S.4.

S12 Brunauer, Emmett and Teller (BET) isotherms

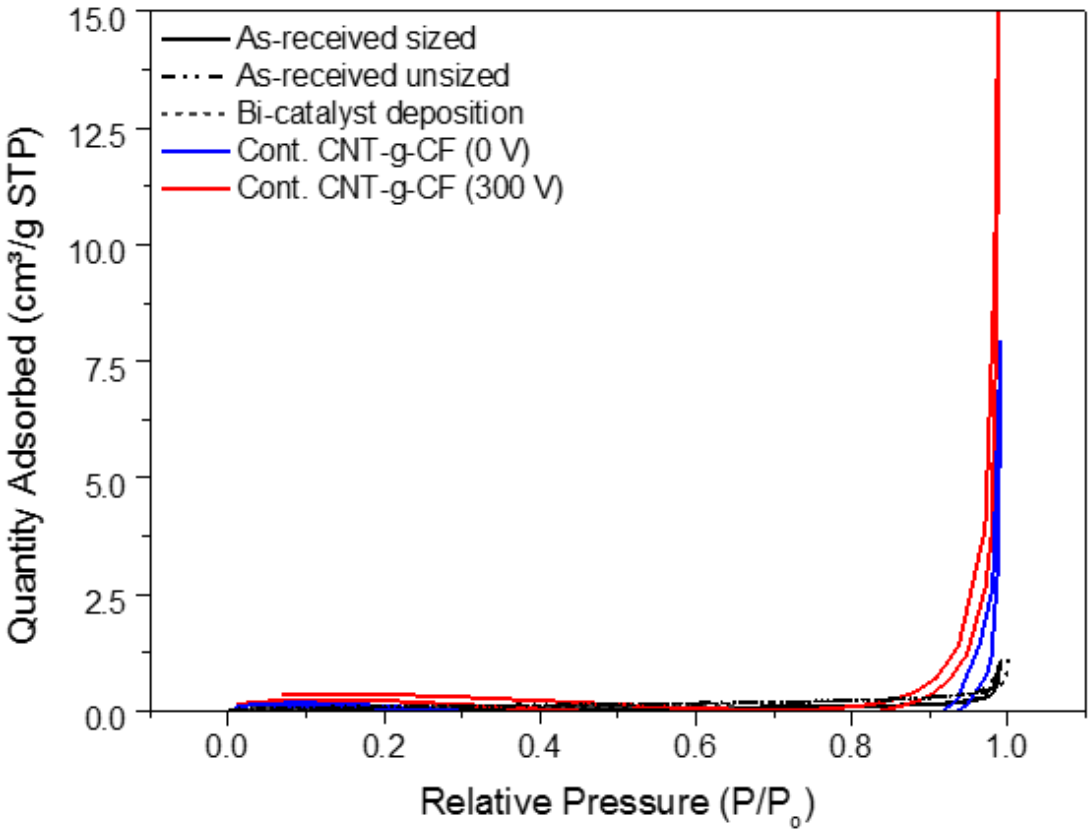

Figure S.15 BET isotherms preformed with nitrogen.

S13 Raman analysis

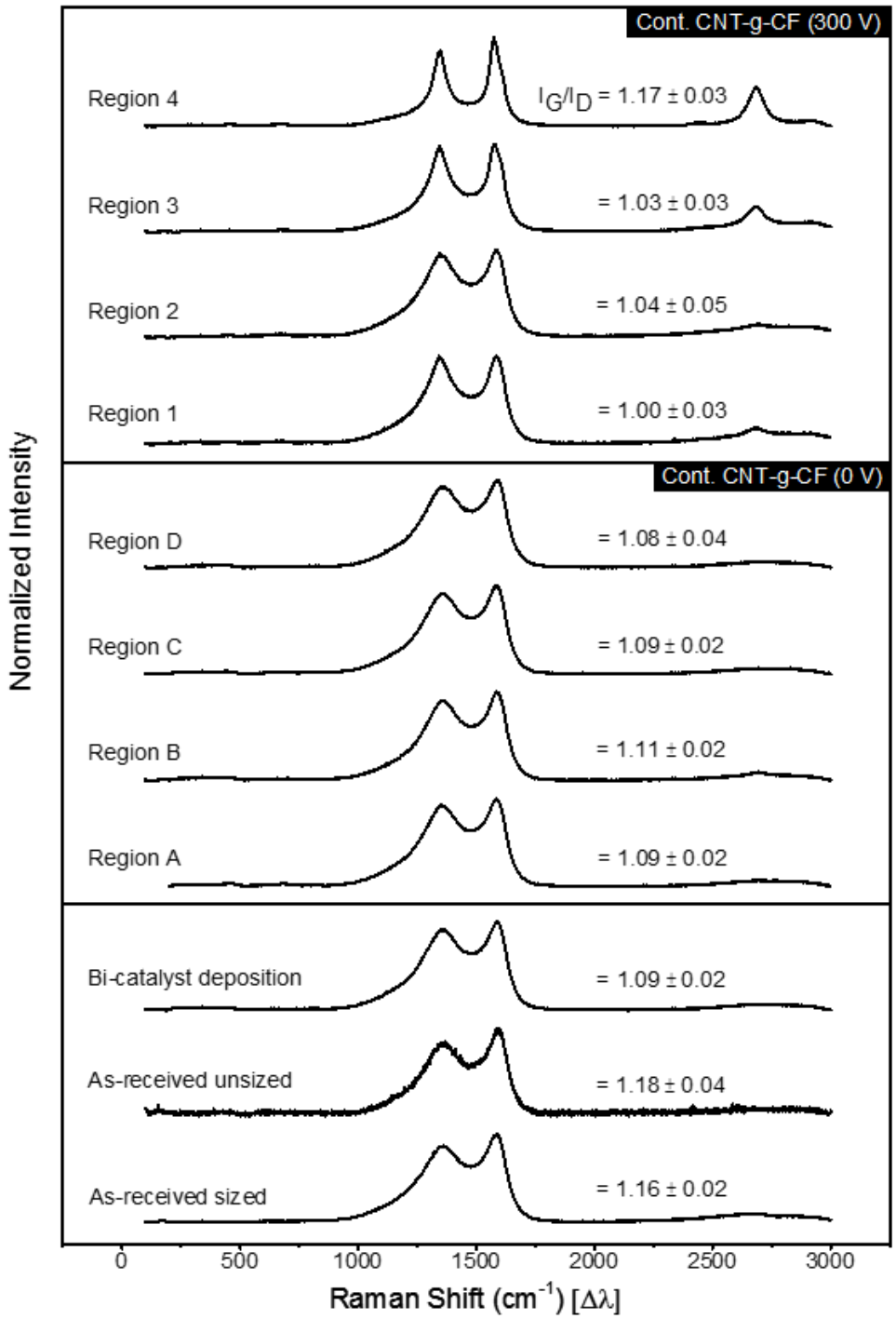

Figure S.16 Raman spectra of as-received sized carbon fiber,[6] as-received unsized carbon fiber, bi-catalyst precursor deposited carbon fiber,[6] and continuously synthesized CNT-g-CF without (0 V) and with (300 V) an applied potential difference with corresponding intensity ratio of the G-mode to the D-mode (I_G/I_D). Various positions are indicated for samples that passed completely through the continuous CVD reactor, with the same Regions 1 to 4, and A to D, of those imaged via SEM in Figure S.6 and Figure S.7, respectively.

S14 Thermogravimetric analysis and derivatives

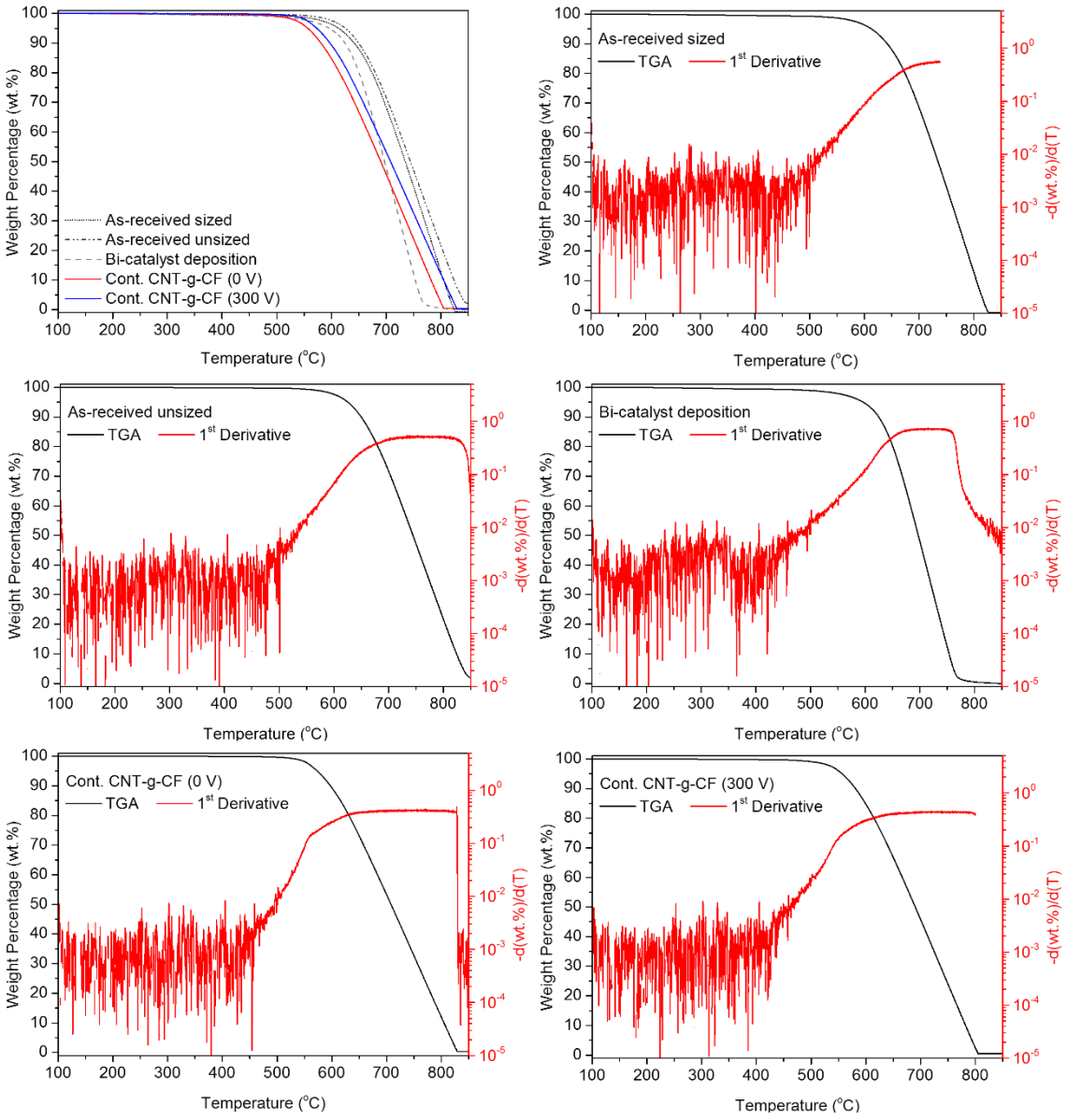

Figure S.17 Thermogravimetric analysis of samples and 1st derivatives (heated in air), with as-received sized and bi-catalyst precursor deposited carbon fiber presented previously.[6]

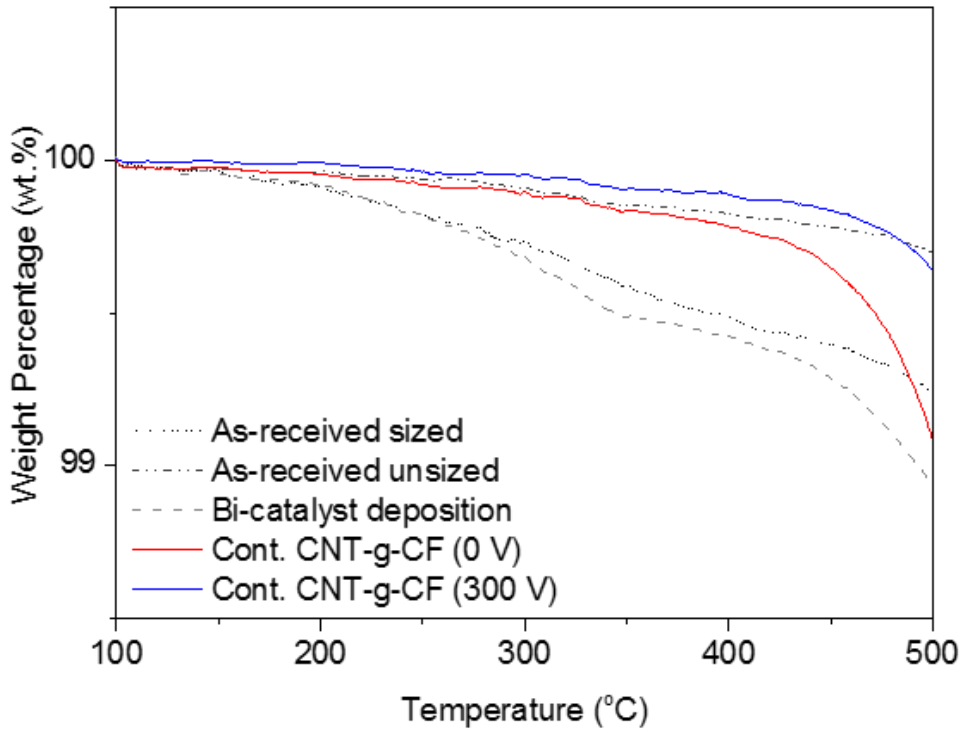

Figure S.18 Thermogram of samples heated in air, with a close up of the temperature region between 100 °C to 500 °C. As-received sized and bi-catalyst precursor deposited carbon fiber presented previously.[6]

S14.1 Determining temperature combustion onset

Onset combustion temperature, provided in Table 2 in the main text, was determined when the thermogram's derivative deviates from the noise for five consecutive measurements.

S15 Continuous CVD carbon nanotube-grafted-carbon fiber with sequentially altered potential difference

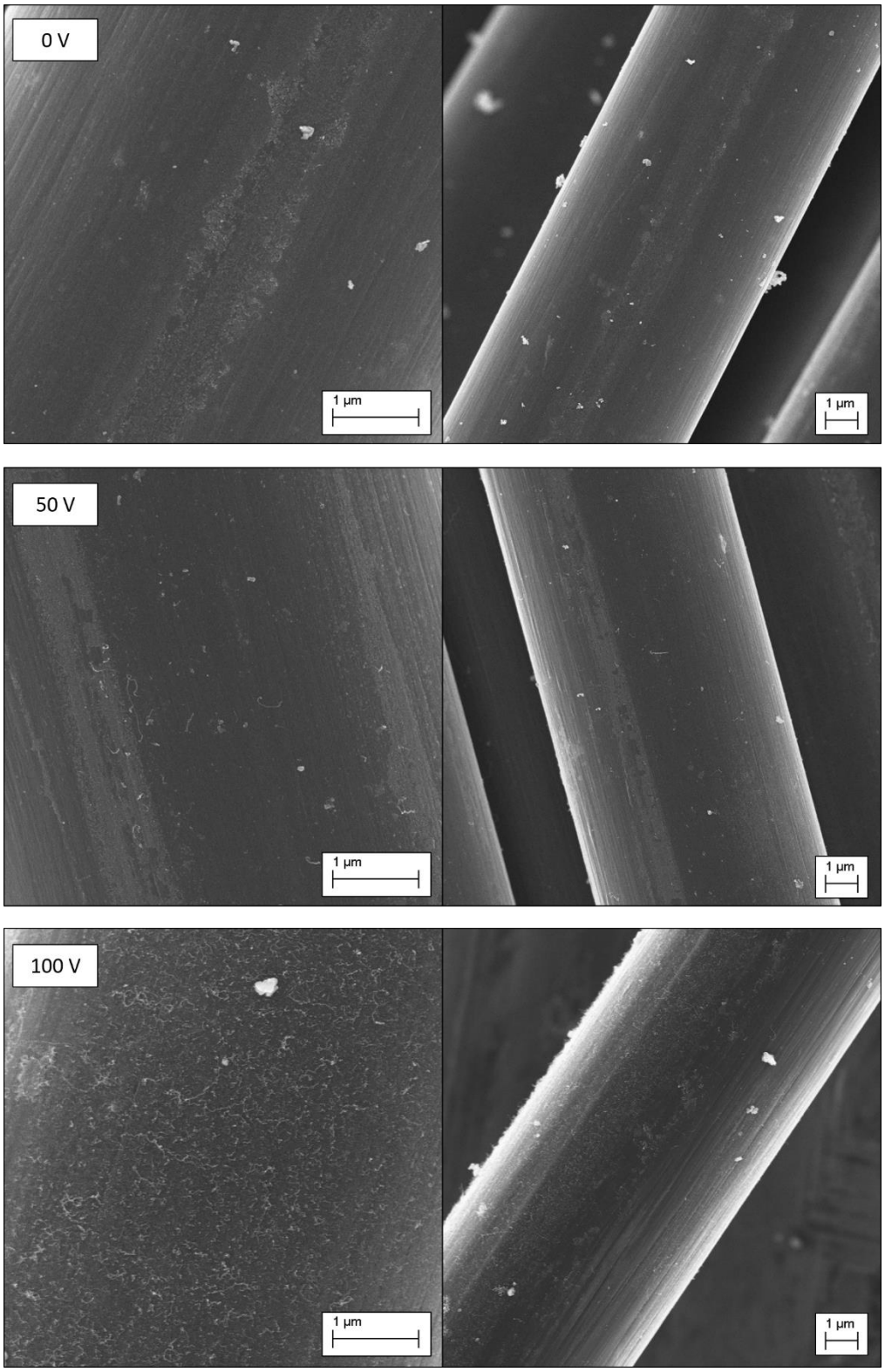

Figure S.19 SEM images of Continuous CVD CNT-g-CF with sequentially increased potential difference starting from 0 V (series continued in Figure S.20).

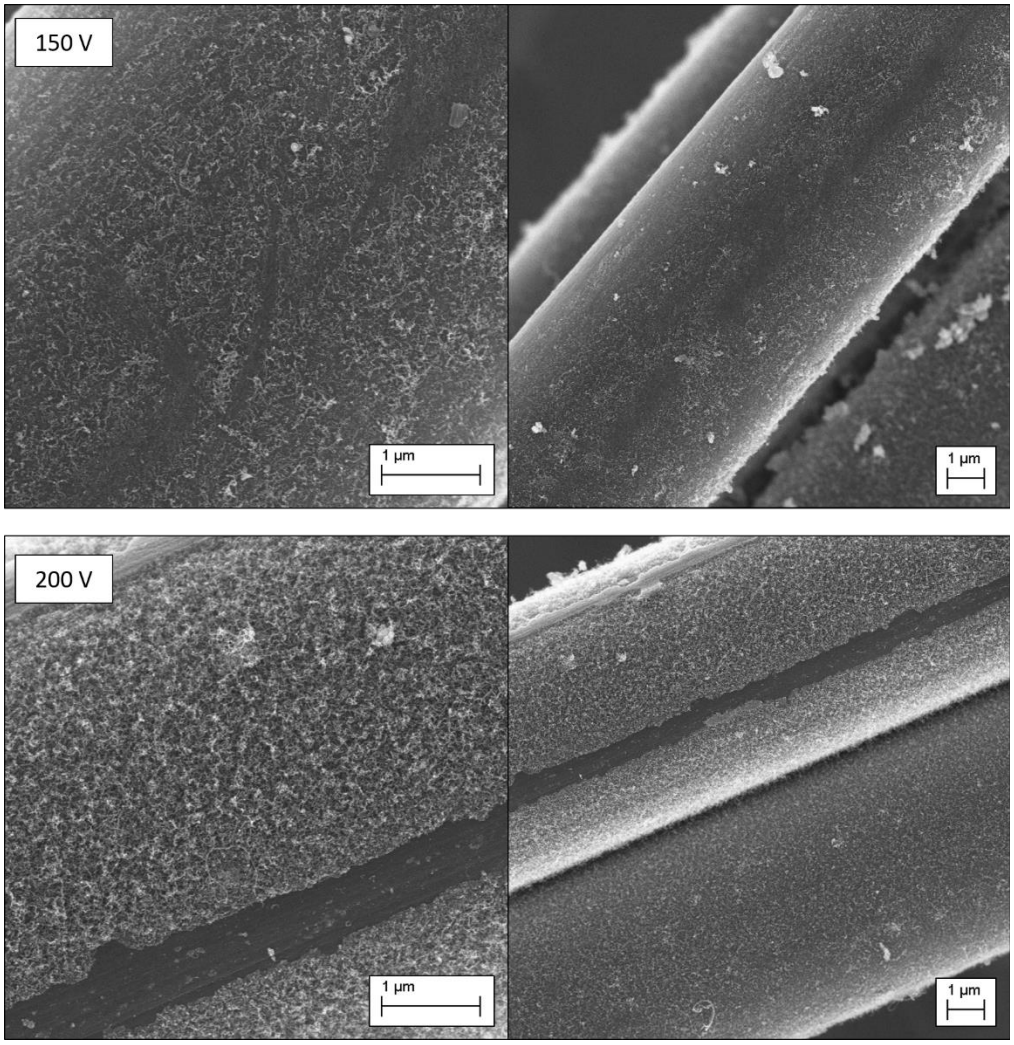

Figure S.20 SEM images of Continuous CVD CNT-g-CF with sequentially increased potential difference starting from 0 V (continued from Figure S.19).

Appendix acronyms and symbols

Adiabatic flame temperature at constant pressure, zero-Tci Temp
Atmospheric pressure, atm
Auto ignition temperature, AIT
Boiling point, BP
Brunauer, Emmett and Teller, BET
Carbon fiber reinforced composite, CFRC
Carbon nanotube-grafted-fiber, CNT-g-F
Carbon nanotube-grafted-carbon fiber, CNT-g-CF
Carbon nanotube, CNT
Chemical vapor deposition, CVD
Critical fiber length, l_c
Distance from fiber-fiber center in a regular hexagonal packing arrangement, A
Embedded fiber length, l_e
Fiber diameter, d
Fiber volume fraction, v_f
Fragmentation failure/pull-out fiber diameter, d_f
Interfacial shear strength, IFSS, τ_i, τ_{app}
Intensity ratio of the G-mode to the D-mode, I_G/I_D
Maximum flammable gas content for which a mixture in nitrogen is not flammable in air, T_{ci}
Outer diameter, OD
Peak pull-out force, $F_{\max}$
Potential difference, p.d.
Radius, r
Scanning electron microscope, SEM
Separation between fibers in a regular hexagonal packing arrangement, B
Standard ambient temperature and atmospheric pressure, SATP
Tensile fiber strength, σ_f
Tensile fiber modulus, E_f, E
Thermal gravimetric analysis, TGA
Transmission electron microscopy, TEM
Ultimate fiber strength at critical length, $\bar{\sigma}_f(l_c)$
Weibull scale parameter, α
Weibull shape parameters/Weibull modulus, β

Acknowledgements

The authors D.B.A., H.D.L., E.R.D., E.S.G., A.B., and M.S.P.S. would like to thank the UK Engineering and Physical Sciences Research Council (EPSRC) (EP/P502500/1), EPSRC Impact Acceleration: Pathways to Impact Award (EP/K503733/1) and Weizmann UK Programme Grant, The Weizmann Institute of Science, Hierarchical composites based on carbon nanotube fibres (2012-2015) for financial support of this work. We thank Hexcel for supplying the AS4C and AS4 carbon fibers. Dr Jodie Melbourne and Dr Adam J. Clancy, NanoHAC Group, Imperial College London are acknowledged for their help with TEM and TGA, respectively. Keith Morley and LewVac LLP, GB and Mr Richard J. Wallington and Chemical Engineering Mechanical Workshop, Imperial College London are acknowledged for consultation and fabrication of the quartz metal fittings and assistance fabricating the line, respectively. H.D.W. and X.M.S. would like to acknowledge partial support from the G.M.J. Schmidt Minerva Centre of Supramolecular Architectures at the Weizmann Institute, and the China-Israel Science Foundations collaborative research grant. This research was also made possible in part by the generosity of the Harold Perlman family. H.D.W. is the recipient of the Livio Norzi Professorial Chair in Materials Science. All underlying data to support the conclusions are provided within the manuscript or supplementary information. Declaration of interest: none.

Appendix references

[1] Molnarne, M.; Mizsey, P.; Schröder, V., Flammability of Gas Mixtures: Part 2: Influence of Inert Gases. Journal of Hazardous Materials 2005, 121 (1-3), 45-49 http://dx.doi.org/10.1016/j.jhazmat.2005.01.033.

[2] CHEMSAFE (BAM), Safety Characteristic Data, Volume 2: Explosion Regions of Gas Mixtures. Wirtschaftsverlag NW - Verlag für neue Wissenschaft: Germany, 2008; p 541, ISBN: 978-3-86509-856-6.

[3] Schröder, V.; Molnarne, M., Flammability of Gas Mixtures: Part 1: Fire Potential. Journal of Hazardous Materials 2005, 121 (1-3), 37-44 http://dx.doi.org/10.1016/j.jhazmat.2005.01.032.

[4] Zabetakis, M. G., Flammability Characteristics of Combustible Gases and Vapors. U.S. Department of the Interior: 1965; Vol. Buletin 627, http://dx.doi.org/10.2172/7328370.

[5] eLearning CERFACS Adiabatic Flame Temperature Calculator. http://elearning.cerfacs.fr/combustion/tools/adiabaticflametemperature/index.php (accessed 09/09/2012), http://elearning.cerfacs.fr/combustion/tools/adiabaticflametemperature/index.php.

[6] Anthony, D. B.; Qian, H.; Clancy, A. J.; Greenhalgh, E. S.; Bismarck, A.; Shaffer, M. S. P., Applying a potential difference to minimise damage to carbon fibres during carbon nanotube grafting by chemical vapour deposition. Nanotechnology 2017, 28 (30), 305602 http://dx.doi.org/10.1088/1361-6528/aa783f.